Brigham Young University
Department of Electrical and Computer Engineering

459 Clyde Building
Provo, Utah 84602

Finite-Aperture Wire Grid Polarizers

Michael A. Jensen
Gregory P. Nordin

30 June 1999

MERS Technical Report # MERS 99-08
ECEN Department Report # TR-J100-99.8

Microwave Earth Remote Sensing (MERS) Laboratory

Finite-Aperture Wire Grid Polarizers

Michael A. Jensen
Department of Electrical and Computer Engineering
459 Clyde Building
Brigham Young University
Provo, UT 84602

Gregory P. Nordin
Department of Electrical and Computer Engineering
University of Alabama, Huntsville
Huntsville, Alabama 35899

Abstract – The transmission characteristics of perfectly conducting wire grid polarizers fabricated in finite and infinite apertures are investigated using a rigorous spectral domain mode-matching method. Specifically, the transmission coefficient for both transverse electric and transverse magnetic polarizations, extinction ratio, and diffraction pattern are characterized for a wide variety of geometrical parameters including aperture dimension, conducting wire fill factor, wire spacing, polarizer thickness, and incident wave arrival angle. The results indicate that the transmission behavior is largely insensitive to aperture dimension.

I. Introduction

Wire grid polarizers have long been recognized as an effective option for discriminating between orthogonal linear polarization states in the infrared portion of the electromagnetic spectrum[1,2]. Such polarizers can be fabricated by placing conducting wires within an aperture formed in a larger opaque screen. When this aperture is electrically large, the device behavior is similar to that of a polarizer of infinite extent, and its performance can be accurately characterized using simulation approaches such as Rigorous Coupled Wave Analysis (RWCA)[3–5]. However, new fabrication technologies and applications that require small-aperture polarizers[6] and arrays of micropolarizers[7,8] have motivated the development of devices with electrically small apertures. In this case, alternative simulation techniques which model the finite aperture extent must be explored for device characterization.

Some recent work has appeared on the subject of simulating finite-aperture diffractive

devices. For example, the boundary element method (BEM) has been shown to be effective in the analysis of finite-number-of-periods (FNP) dielectric and finite-conductivity metallic grating structures[9], diffractive optical lenses[10–12], and other aperiodic structures[13]. Method of moments solution techniques have also been applied to lenslet analysis based upon both rigorous surface[14] and volume[15] integral formulations for the fields. For perfectly conducting gratings, spectral-domain mode-matching solutions appear to be effective[16,17]. While these studies have provided significant insight into the behavior of finite-extent diffractive devices, they have not focused on extending and applying such techniques to perform detailed analyses of finite-aperture wire grid polarizers.

In this paper, we present a detailed characterization of perfectly conducting wire grid polarizers placed in finite apertures. The analysis uses a mode-matching technique in which the fields scattered by the polarizer are expressed using a spectral domain representation[17–20]. The resulting solution allows highly accurate simulations of two-dimensional polarizer structures for both transverse electric (TE) and transverse magnetic (TM) illuminations. The finite aperture case is extended to infinitely long polarizers by using a Floquet mode analysis which exploits periodicity. A large variety of results are presented which illustrate the transmission characteristics of many different polarizer configurations. Effects of aperture dimension, polarizer thickness, wire spacing and fill factor, and optical wave incidence angle are highlighted.

II. TE Illumination

The problem under consideration is that of a plane wave impinging on a finite-sized aperture located in an otherwise infinite conducting plane of thickness $D = 2d$. As indicated in Fig. 1, the aperture is divided into Q slits each of width $w = 2a$, with the qth slit centered at $x = x_q$. The center-to-center spacing of the conducting regions between the slits is denoted as Δx. The wavenumber, permittivity, and permeability in each region are expressed as k_j, ϵ_j, and μ_j respectively, where j indicates the region number as defined in Fig. 1. A time variation of $\exp(-i\omega t)$ is assumed and suppressed.

A. Field Solutions

The starting point in the analysis is the proper expression of the fields in the three regions in Fig. 1. For a TE polarized wave, the fields in region 0 can be represented as the sum of incident, reflected, and scattered components which may each be expressed as

$$E_y^i(x,z) = \exp\left[ik_x x - ik_z(z-d)\right] \tag{1}$$

$$E_y^r(x,z) = -\exp\left[ik_x x + ik_z(z-d)\right] \tag{2}$$

$$E_y^s(x,z) = \frac{1}{2\pi}\int_{-\infty}^{\infty} \tilde{E}_y^s(\xi)\exp\left[-i\xi x + i\sqrt{k_0^2-\xi^2}(z-d)\right]d\xi \tag{3}$$

$$\tilde{E}_y^s(\xi) = \int_{-\infty}^{\infty} E_y^s(x,d)\exp\left(i\xi x\right)dx \tag{4}$$

where $k_x = k_0\sin\theta$ and $k_z = k_0\cos\theta$. The spectral representation in Eq. (3) for the scattered field will facilitate later enforcement of continuity conditions along the planes $z = \pm d$. In a similar fashion, the field transmitted into region 2 may be expressed as

$$E_y^t(x,z) = \frac{1}{2\pi}\int_{-\infty}^{\infty} \tilde{E}_y^t(\xi)\exp\left[-i\xi x - i\sqrt{k_2^2-\xi^2}(z+d)\right]d\xi \tag{5}$$

$$\tilde{E}_y^t(\xi) = \int_{-\infty}^{\infty} E_y^t(x,-d)\exp\left(i\xi x\right)dx. \tag{6}$$

Finally, the fields in the qth slit in region 1 can be expressed using modes which satisfy the boundary conditions on the slit sidewalls. This results in the summation

$$E_y^q(x,z) = \sum_{n=1}^{\infty}\left(b_n^q\cos\zeta_n z + c_n^q\sin\zeta_n z\right)\sin\left[a_n\left(x - x_q + a\right)\right] \tag{7}$$

where $a_n = n\pi/2a$ and $\zeta_n = \sqrt{k_1^2 - a_n^2}$.

Using these field representations, we must now enforce continuity of tangential fields at $z = \pm d$ and solve for unknown quantities. For convenience, we will define the functions

$$G_{1,2}(m,\xi) = \frac{(-1)^m\exp\left(\mp i\xi a\right) - \exp\left(\pm i\xi a\right)}{\xi^2 - a_m^2} \tag{8}$$

where the top and bottom signs are for G_1 and G_2 respectively. Following the procedure outlined in[17], enforcing continuity of E_y leads to the expressions

$$\tilde{E}_y^{s,t}(\xi) = \sum_{q=1}^{Q}\sum_{n=1}^{\infty}\left(b_n^q\cos\zeta_n d \pm c_n^q\sin\zeta_n d\right)a_n G_2(n,\xi)\exp\left(i\xi x_q\right) \tag{9}$$

where here, as well as in other equations in this paper, the upper and lower signs are used for scattered and transmitted fields respectively. Now, using the relation $H_x = (i/\omega\mu)\partial E_y/\partial z$, we can enforce continuity of the magnetic fields over each slit. If we then approximate the infinite series in Eq. (9) using the first N terms and order the unknowns b_n^q and c_n^q into column vectors B and C, we obtain the block-matrix equation

$$\begin{bmatrix} \Psi_{0B} & \Psi_{0C} \\ \Psi_{2B} & -\Psi_{2C} \end{bmatrix} \begin{bmatrix} B \\ C \end{bmatrix} = \begin{bmatrix} \Gamma \\ 0 \end{bmatrix} \tag{10}$$

where

$$\Psi_{lB,rs} = \zeta_m a \frac{\mu_l}{\mu_1} \sin\zeta_m d \ \delta_{rs} + \frac{i a_n a_m}{2\pi} \cos\zeta_n d \ \ I_{mnpq}(k_l) \tag{11}$$

$$\Psi_{lC,rs} = -\zeta_m a \frac{\mu_l}{\mu_1} \cos\zeta_m d \ \delta_{rs} + \frac{i a_n a_m}{2\pi} \sin\zeta_n d \ \ I_{mnpq}(k_l) \tag{12}$$

$$\Gamma_r = 2k_z a_m G_2(m, k_x) \exp(i k_x x_p) \tag{13}$$

and $r = (p-1)N + m$, $s = (q-1)N + n$. The integral $I_{mnpq}(k)$ is expressed as

$$I_{mnpq}(k_l) = \int_{-\infty}^{\infty} G_1(m,\xi) G_2(n,\xi) \sqrt{k_l^2 - \xi^2} \exp\left[i\xi(x_q - x_p)\right] d\xi. \tag{14}$$

A technique for efficient evaluation of this integral is provided in Appendix A.

B. Far-Fields and Transmission Coefficient

Solution of Eq. (10) allows determination of the unknown coefficients b_n^q and c_n^q which can subsequently be used to determine fields using Eqs. (3), (5), (7), and (9). For far-zone observations, we can let $x = r_s \sin\theta_s$ and $z - d = r_s \cos\theta_s$ for $z \geq d$, and $x = r_t \sin\theta_t$ and $z + d = -r_t \cos\theta_t$ for $z \leq -d$. Then, using the method of steepest descent for $r_{s,t}$ large, we manipulate Eqs. (3) and (5) into the general expression

$$\begin{aligned} E_y^{s,t}(\theta_{s,t}) = & \sqrt{\frac{k_{0,2}}{i2\pi r_{s,t}}} \cos\theta_{s,t} \sum_{q=1}^{Q} \sum_{n=1}^{N} a_n \left(b_n^q \cos\zeta_n d \pm c_n^q \sin\zeta_n d\right) \\ & \times G_1(n, k_{s,t}) \exp\left[i(k_{0,2} r_{s,t} - k_{s,t} x_q)\right] \end{aligned} \tag{15}$$

where $k_s = k_0 \sin\theta_s$ and $k_t = k_2 \sin\theta_t$.

The transmission coefficient of the polarizer is defined as the ratio of the total power transmitted by the aperture to that intercepted by the aperture. This corresponds to placing

a detector behind the polarizer such that it captures all of the transmitted light. In order to maintain consistency for comparisons performed later in this paper, the aperture dimension is taken to be $Q\Delta x$. Using this convention leads to the expression

$$\begin{aligned} T &= \frac{1}{Qk_0\cos\theta}\frac{a}{\Delta x}\frac{\mu_0}{\mu_1}\sum_{q=1}^{Q}\sum_{n=1}^{N}\mathrm{Im}\left\{\zeta_n^*\left(b_n^q\cos\zeta_n d - c_n^q\sin\zeta_n d\right)\right. \\ &\quad \left.\times\left(b_n^q\sin\zeta_n d + c_n^q\cos\zeta_n d\right)^*\right\}. \end{aligned} \tag{16}$$

C. Infinite Periodic Structure

In the event that the number of apertures Q becomes infinite, the solution methodology can be altered to allow efficient evaluation of the fields. In this case, the fields in regions 0 and 2 are expressed in terms of Floquet harmonics,

$$E_y^{s,t}(x,z) = \sum_{p=-\infty}^{\infty}\gamma_p^{s,t}\exp\left[-i\xi_p x \pm i\sqrt{k_{0,2}^2-\xi_p^2}(z\mp d)\right] \tag{17}$$

$$\gamma_p^{s,t} = \frac{1}{\Delta x}\int_{-\Delta x/2}^{\Delta x/2}E_y^{s,t}(x,\pm d)\exp\left(i\xi_p x\right)dx \tag{18}$$

where $\xi_p = k_x + 2\pi p/\Delta x$.

With this representation, the problem becomes that of finding the fields in a single aperture ($Q=1$). Enforcement of tangential field continuity leads to the expression

$$\gamma_p^{s,t} = \frac{1}{\Delta x}\sum_{n=1}^{\infty}\left(b_n\cos\zeta_n d \pm c_n\sin\zeta_n d\right)a_n G_2(n,\xi_p) \tag{19}$$

as well as a matrix equation of the form of Eq. (10) with elements

$$\Psi_{lB,mn} = \zeta_m a\frac{\mu_l}{\mu_1}\sin\zeta_m d\ \delta_{mn} + \frac{ia_n a_m}{\Delta x}\cos\zeta_n d\ \ F_{mn}(k_l) \tag{20}$$

$$\Psi_{lC,mn} = -\zeta_m a\frac{\mu_l}{\mu_1}\cos\zeta_m d\ \delta_{mn} + \frac{ia_n a_m}{\Delta x}\sin\zeta_n d\ \ F_{mn}(k_l) \tag{21}$$

and with Γ_m given in Eq. (13). It is noteworthy that this matrix equation has dimension $N\times N$, in contrast to the $QN\times QN$ equation encountered for the finite-aperture case. The terms F_{mn} are given by the rapidly converging sum

$$F_{mn}(k_l) = \sum_{p=-\infty}^{\infty}G_1(m,\xi_p)G_2(n,\xi_p)\sqrt{k_l^2-\xi_p^2}. \tag{22}$$

At this point, computation of the transmission coefficient may be performed using the expression in Eq. (16) with $Q = 1$. However, when placing Eq. (19) into Eq. (17), it should be noted that only a finite number of series terms will be characterized by propagation in the $\pm z$ directions. These terms represent plane waves which will propagate to the far-zone. For the wire spacings typical in polarizer applications, only the $p = 0$ term will propagate to the far-field.

III. TM Illumination

A. Field Solutions

The analysis of a TM polarized plane wave parallels that of the TE polarization investigated above. Expression of the fields in this case can be performed simply by replacing the symbol E with H in Eqs. (1)–(6) to indicate we are working with magnetic fields. For the fields in the qth slit, however, we must alter the series expansion to the form

$$H_y^q(x,z) = \sum_{n=0}^{\infty} \left(b_n^q \cos\zeta_n z + c_n^q \sin\zeta_n z\right) \cos\left[a_n\left(x - x_q + a\right)\right] \tag{23}$$

in order to satisfy proper boundary conditions in the slit.

With these representations, we first use the relation $E_x(x,z) = (1/i\omega\epsilon)\partial H_y/\partial z$ and then enforce electric field continuity at $z = \pm d$ to obtain the equations

$$\tilde{E}_x^{s,t}(\xi) = \frac{1}{\omega\epsilon_1} \sum_{q=1}^{Q} \sum_{n=0}^{\infty} \zeta_n \left(\pm b_n^q \sin\zeta_n d - c_n^q \cos\zeta_n d\right) \xi G_2(n,\xi) \exp\left(i\xi x_q\right). \tag{24}$$

Truncating this series to the first N terms, enforcing continuity of tangential magnetic fields at each slit, and utilizing the relations

$$\tilde{E}_x^{s,t}(\xi) = \pm\frac{1}{\omega\epsilon_{0,2}}\sqrt{k_{0,2}^2 - \xi^2}\,\tilde{H}_y^{s,t}(\xi) \tag{25}$$

results in a block-matrix equation identical in form to that of Eq. (10). In this case, the matrix elements assume the form

$$\Psi_{lB,rs} = \sigma_m a \cos\zeta_m d\ \delta_{rs} - \frac{i}{2\pi}\frac{\epsilon_l}{\epsilon_1}\zeta_n \sin\zeta_n d\ \ I_{mnpq}(k_l) \tag{26}$$

$$\Psi_{lC,rs} = \sigma_m a \sin\zeta_m d\ \delta_{rs} + \frac{i}{2\pi}\frac{\epsilon_l}{\epsilon_1}\zeta_n \cos\zeta_n d\ \ I_{mnpq}(k_l) \tag{27}$$

$$\Gamma_r = -i2k_x G_2(m,k_x) \exp\left(ik_x x_p\right) \tag{28}$$

where $\sigma_0 = 2$, $\sigma_m = 1$ for $m > 0$, and

$$I_{mnpq}(k_l) = \int_{-\infty}^{\infty} G_1(m,\xi) G_2(n,\xi) \frac{\xi^2}{\sqrt{k_l^2 - \xi^2}} \exp\left[i\xi(x_q - x_p)\right] d\xi. \tag{29}$$

B. Far-Fields and Transmission Coefficient

Using the procedure outlined above for the TE case, the far-zone scattered and transmitted fields assume the form

$$\begin{aligned} H_y^{s,t}(\theta_{s,t}) &= -\frac{\epsilon_{0,2}}{\epsilon_1} \sqrt{\frac{k_{0,2}}{i2\pi r_{s,t}}} \sin\theta_{s,t} \sum_{q=1}^{Q} \sum_{n=0}^{N-1} \zeta_n \left(b_n^q \sin\zeta_n d \mp c_n^q \cos\zeta_n d\right) \\ &\quad \times G_1(n, k_{s,t}) \exp\left[i(k_{0,2} r_{s,t} - k_{s,t} x_q)\right]. \end{aligned} \tag{30}$$

The transmission coefficient is given as

$$\begin{aligned} T &= \frac{-1}{Qk_0 \cos\theta} \frac{a}{\Delta x} \frac{\epsilon_0}{\epsilon_1} \sum_{q=1}^{Q} \sum_{n=0}^{N-1} \mathrm{Im}\left\{\sigma_n \zeta_n \left(b_n^q \sin\zeta_n d + c_n^q \cos\zeta_n d\right)\right. \\ &\quad \left. \times \left(b_n^q \cos\zeta_n d - c_n^q \sin\zeta_n d\right)^*\right\}. \end{aligned} \tag{31}$$

C. Infinite Periodic Structure

For the infinite aperture case, we can use the field representations in Eqs. (17) and (18) with the symbol E replaced with H. Enforcement of tangential field continuity leads to the expression

$$\gamma_p^{s,t} = \frac{1}{\Delta x \sqrt{k_{0,2}^2 - \xi_p^2}} \frac{\epsilon_{0,2}}{\epsilon_1} \sum_{n=1}^{\infty} \zeta_n \left(b_n \sin\zeta_n d \mp c_n \cos\zeta_n d\right) \xi_p G_2(n, \xi_p) \tag{32}$$

as well as a matrix equation of the form of Eq. (10) with elements

$$\Psi_{lB,mn} = \sigma_m a \cos\zeta_m d \ \delta_{mn} - \frac{i}{\Delta x} \frac{\epsilon_l}{\epsilon_0} \sin\zeta_n d \ \ F_{mn}(k_l) \tag{33}$$

$$\Psi_{lC,mn} = \sigma_m a \sin\zeta_m d \ \delta_{mn} + \frac{i}{\Delta x} \frac{\epsilon_l}{\epsilon_0} \cos\zeta_n d \ \ F_{mn}(k_l) \tag{34}$$

and with Γ_m given in Eq. (28) (with $x_p = 0$). The terms F_{mn} are given by the sum

$$F_{mn}(k_l) = \sum_{p=-\infty}^{\infty} G_1(m, \xi_p) G_2(n, \xi_p) \frac{\xi_p^2}{\sqrt{k_l^2 - \xi_p^2}}. \tag{35}$$

Again, computation of the transmission coefficient may be performed using the expression in Eq. (31) with $Q = 1$.

IV. Results

In this section, we utilize the theory developed in Sections II and III to investigate the behavior of the wire grid polarizer for different geometrical parameters and incident wave characteristics. Throughout the discussion, the following terms will be utilized to quantify the device parameters:

Fill Factor:	$1 - \mathrm{w}/\Delta x$
Aperture Size:	$Q\Delta x$
Slit Density (number of slits/wavelength):	$\lambda/\Delta x$
Extinction Ratio:	T_{TM}/T_{TE}

where the subscripts on the transmission coefficient (T) denote the polarization.

To validate the theoretical model used in the investigation, transmission coefficient and diffraction pattern results generated for several different single- and multiple-slit structures were compared with cases shown in the literature[17-21]. In every case, the results of the present analysis agreed with other published results. The extensive validation performed provides confidence that the method will accurately simulate the behavior of the optical fields in the polarizer structures under investigation.

A. Transmission Coefficient and Extinction Ratio

To begin our study, we investigate the behavior of the polarizer transmission coefficient for different geometrical configurations. In this investigation, it is important to emphasize that the transmission coefficient is defined as the ratio of the total power transmitted to the total power *intercepted* by the polarizer aperture. In the following discussion of Figs. 2–8, each figure has parts (a) and (b) which show the transmission coefficient for both TM and TE polarizations and the extinction ratio, respectively. Unless otherwise indicated, all plots are for normally incident illumination ($\theta = 0°$).

As a starting point, consider Fig. 2 which shows the transmission behavior as a function of aperture size for several different values of the fill factor for an infinitesimally thin polarizer

($D = 0$). The computations assume 5 slits/λ ($\Delta x = 0.2\lambda$), and $N = 5$ modes to describe the fields within each slit. These plots demonstrate that while very small apertures tend to have somewhat reduced transmission coefficient values, the transmission and extinction characteristics of apertures with dimensions greater than about 1λ are relatively insensitive to aperture size. The results also indicate that as the fill factor is increased, the transmission coefficient for both polarizations decreases due to the increased area occupied by the conducting wire. Additionally, an increased fill factor improves the extinction ratio[22], indicating that the transmission coefficient for the TE polarization is more significantly influenced by the increase in conductor size. It should be mentioned that the infinite aperture analysis outlined above predicts transmission coefficients of 0.999, 0.991, and 0.953 for TM and 0.162, 0.040, and 0.007 for TE for fill factors of 0.2, 0.4, and 0.6 respectively. Examination of the curves in Fig. 2 (a) reveals that the results from the finite aperture computation approach these values as the aperture dimension increases.

Fig. 3 depicts the polarizer transmission behavior as a function of the slit density for an infinitesimally thin polarizer again for three values of the fill factor. These results illustrate that the previously observed fill factor trends remain the same as the slit density is varied. These plots also demonstrate that as the slit density is increased, the transmission coefficient for the TM polarization increases toward unity while that for the TE polarization rapidly decreases toward zero, resulting in a substantial increase in the extinction ratio. This behavior is consistent with expectation since an increase in slit density implies an increased number of thinner, more closely-spaced wires. Such a distribution of the conductor in the aperture tends to be less disruptive to the TM polarization and more disruptive to the TE polarization.

This conclusion is reinforced by the curves in Fig. 4 which show the transmission characteristics as a function of slit density for three different aperture sizes. But perhaps more evident in this figure is the insensitivity of the polarizer behavior to aperture size. This is particularly dramatic in Fig. 4 (b) which shows very little difference in the extinction ratio whether the aperture size is 1λ or infinite in extent.

The parametric studies discussed above assume an infinitesimally thin polarizer. However, in practical polarizer configurations, the wire aspect ratio (and therefore thickness) is an issue which impacts both the performance[23] and the fabrication of the device. For example, Fig. 5 shows the transmission behavior as a function of aperture size for four different values of the thickness D. These results indicate that the polarizer characteristics remain relatively insensitive to aperture dimension even for the finite-thickness case. They also demonstrate that increasing the conductor thickness decreases the transmission coefficient for both polarizations yet noticeably increases the extinction ratio. This effect can be explained by considering that the narrow, finite-thickness slit represents a parallel-plate waveguide which supports only the lowest order transverse electromagnetic (TEM) mode. Since the TM wave is properly polarized to excite this TEM mode, it passes through relatively easily with reflections due mainly to the impedance mismatch between the incident plane wave and the propagating mode. However, the TE waveguide modes excited by the incident TE plane wave will be cut off, and therefore TE transmission falls off dramatically with D. Also noteworthy in this plot is the oscillation present in the TM transmission coefficient for larger conductor thicknesses.

Fig. 6, which shows the transmission behavior as a function of fill factor for four values of thickness, further illustrates the reduction in transmission coefficient and increase in extinction ratio with increasing polarizer thickness. These results also demonstrate the dramatic decrease in transmission power commensurate with large values of the fill factor as well as the accentuation of this roll off as the polarizer thickness is increased. This is further illustrated in Fig. 7 in which the transmission characteristics are shown as a function of polarizer thickness parameterized by the fill factor. For a given fill factor, the extinction ratio increases significantly with polarizer thickness.

Many applications require both large extinction ratio and high optical throughput. Based on the above results, the extinction ratio can, in general, be augmented by increasing either the slit density, fill factor, thickness, or some combination of these parameters. However, a high optical throughput is achieved with a low fill factor, or, if the fill factor is constrained

to be large, by decreasing the polarizer thickness. Clearly, designing a wire grid polarizer for a particular application involves distinct trade-offs between the extinction ratio and optical throughput.

Fabrication considerations impose additional constraints on wire grid polarizer design. For example, consider the use of microfabrication techniques to create a polarizer for the infrared or visible portion of the spectrum. Minimum feature size limitations determine the maximum slit density and affect the fill factor, which in turn influence the extinction ratio. Whether the wires are formed with an etch[8,22] or lift-off process, wire aspect ratio considerations affect the selection of polarizer thickness. Hence wire grid polarizer design involves making careful tradeoffs between application requirements and physical and fabrication constraints.

Before concluding this section, we also consider the polarizer transmission properties as a function of the incidence angle. Fig. 8 shows the effect of incidence angle for several different aperture sizes. Because of the non-zero grating thickness ($D = 0.1\lambda$), the TE transmission power is very small for all angles and apertures. It should be emphasized that the transmission coefficient has been normalized by $\cos\theta$ to accurately show the behavior near $\theta = 90°$ where the denominator of T goes to zero. The fact that the finite-sized apertures have a non-zero normalized transmission coefficient for the TM polarization at $\theta = 90°$ implies that fields are transmitted despite the fact that no power is *normally* incident on the structure. However, very little power is transmitted for the TE polarization in this case, resulting in the very large extinction ratio observed.

B. Diffraction Pattern

Another important characteristic of finite aperture polarizers is the angular distribution of the transmitted energy for the TM polarization. In this section, the polarizer diffraction pattern is presented as the ratio of the transmitted power density to the power density that would be obtained if the power intercepted by the aperture were radiated isotropically into the space $z < -d$. Mathematically, this is given as

$$G_t(\theta_t) \;=\; 10\log\left[\frac{\eta_2|H_y^t(\theta_t)|^2/2}{P_i/\pi r_t}\right]$$

$$= \quad 10 \log \left[\frac{\eta_2}{\eta_0} \frac{|H_y^t(\theta_t)|^2}{|H_i|^2} \frac{\pi r_t}{Q \Delta x \cos\theta} \right] \tag{36}$$

where P_i is the power intercepted by the aperture.

Fig. 9 shows the diffraction pattern for three different aperture sizes. As expected, the diffraction pattern is highly sensitive to the aperture dimension. Fig. 10 illustrates the effect of polarizer thickness on the radiation characteristics. Clearly, thickness exercises only a marginal influence on the pattern, with the most notable effects being present in the wide angular regions where the transmitted power concentration is small. Finally, Fig. 11 illustrates the diffraction pattern for different arrival angles of the incident plane wave. These curves reveal the expected shift in the main beam direction to match that of the incident wave as well as a decrease in power in the main radiation lobe and an increase in the sidelobes.

V. Summary

This paper has provided a detailed examination of the transmission characteristics of perfectly conducting, finite-aperture wire grid polarizers. The analysis approach consisted of a rigorous mode-matching solution coupled with a spectral representation of the scattered fields. An extension to this theory which incorporated Floquet analysis allowed simulation of infinitely large, periodic polarizers as well. This analysis methodology was used to investigate the transmission coefficient for both TM and TE polarizations, the extinction ratio, and the diffraction pattern for a wide variety of geometrical configurations and incident field characteristics. These studies reveal that for apertures larger than approximately one wavelength, the transmission coefficient and extinction characteristics are largely insensitive to aperture dimension. Also demonstrated was a decrease in transmission coefficient for both polarizations and an increase in extinction ratio with increasing fill factor or increasing thickness. This in turn leads to a trade-off between the achievable optical transmission and extinction ratio. Directions for future research include extending the analysis to finite conductivity wire grid arrays and examining the effects of fabrication-related defects and nonuniformities such as sidewall roughness and fill factor variations.

A Evaluation of I_{mnpq}

Expansion of the integrands in Eqs. (14) and (29) reveals that the integrations may be written as

$$I_{mnpq}(k_l) = \sum_{j=1}^{3} A_{j,mn} T^{(j)}_{mnpq}(k_l) = \sum_{j=1}^{3} A_{j,mn} \int_{-\infty}^{\infty} \frac{f(\xi)}{(\xi^2 - a_m^2)(\xi^2 - a_n^2)} \exp\left(i\beta_{j,pq}\xi\right) d\xi \tag{37}$$

where

$$\begin{aligned} A_{1,mn} &= (-1)^{m+n} + 1 & \beta_{1,pq} &= x_q - x_p \\ A_{2,mn} &= (-1)^{n+1} & \beta_{2,pq} &= x_q - x_p + 2a \\ A_{3,mn} &= (-1)^{m+1} & \beta_{3,pq} &= x_q - x_p - 2a. \end{aligned} \tag{38}$$

and

$$f(\xi) = \begin{cases} \sqrt{k_l^2 - \xi^2} & \text{TE illumination} \\ \dfrac{\xi^2}{\sqrt{k_l^2 - \xi^2}} & \text{TM illumination.} \end{cases} \tag{39}$$

Each of the three integrals $T^{(j)}_{mnpq}$ may be performed using complex integration procedures to obtain

$$T^{(j)}_{mnpq}(k_l) = R^{(j)}_{mnpq}(k_l) + B^{(j)}_{mnpq}(k_l) \tag{40}$$

where $R^{(j)}_{mnpq}$ and $S^{(j)}_{mnpq}$ represent the contributions from the residues and from integrating along the branch cut at $\xi = k_l$, respectively. The residue contributions may be written as

$$R^{(j)}_{mnpq}(k_l) = -\frac{\pi}{a_m^2 - a_n^2} \left[\tau_m \sin\left(\beta_{j,pq} a_m\right) - \tau_n \sin\left(\beta_{j,pq} a_n\right)\right] \tag{41}$$

where

$$\tau_m = \begin{cases} \dfrac{\sqrt{1 - \gamma_m^2}}{\gamma_m} & \text{TE illumination} \\ \dfrac{\gamma_m}{\sqrt{1 - \gamma_m^2}} & \text{TM illumination} \end{cases} \tag{42}$$

and $\gamma_m = a_m / k_l$. The contribution from the branch cut integration becomes

$$B^{(j)}_{mnpq}(k_l) = \frac{i2}{k_l^2} \int_0^{\infty} \frac{g(v) \exp\left[\beta_{j,pq} k_l (i - v)\right]}{\left[(1 + iv)^2 - \gamma_m^2\right]\left[(1 + iv)^2 - \gamma_n^2\right]} dv \tag{43}$$

where

$$g(v) = \begin{cases} \sqrt{v(v-i2)} & \text{TE illumination} \\ \dfrac{(1+iv)^2}{\sqrt{v(v-i2)}} & \text{TM illumination.} \end{cases} \tag{44}$$

Since $\beta_{1,pp} = 0$, $B^{(1)}_{mnpp}$ can be evaluated in closed-form, resulting in the expression

$$B^{(1)}_{mnpp}(k_l) = \pm \frac{i2}{a_m^2 - a_n^2} \left[\tau_m \sin^{-1} \gamma_m - \tau_n \sin^{-1} \gamma_n \right] \tag{45}$$

where the top and bottom signs are used for TE and TM illuminations, respectively. Note that when $m = n$, l'Hôpital's rule must be used to evaluate Eqs. (41) and (45).

REFERENCES

1. G. R. Bird and M. Parrish, Jr., "The wire grid as a near-infrared polarizer," J. Opt. Soc. Am. **50,** 886–891 (1960).
2. J. B. Young, H. A. Graham, and E. W. Peterson, "Wire grid infrared polarizer," Appl. Opt. **4,** 1023–1026 (1965).
3. M. G. Moharam and T. K. Gaylord, "Rigorous coupled-wave analysis of metallic surface-relief gratings," J. Opt. Soc. Am. A **3,** 1780–1787 (1986).
4. E. N. Glytsis and M. G. Moharam, "Rigorous coupled-wave analysis and applications of grating diffraction," In *Diffractive and Miniaturized Optics*, S. H. Lee, ed., Critical Reviews **CR49,** 3–31 (Society of Photo-Optical Instrumentation Engineers, Bellingham, Wash., 1993).
5. M. G. Moharam, E. B. Grann, D. A. Pommet, and T. K. Gaylord, "Formulation for stable and efficient implementation of the Rigorous Coupled-Wave Analysis of Binary Gratings," J. Opt. Soc. Am. A **12,** 1068–1076 (1995).
6. E. Chen and S. Y. Chou, "A novel device for detecting the polarization direction of linear polarized light using integrated subwavelength gratings and photodetectors," IEEE Phot. Tech. Lett. **9,** 1259–1261 (1997).
7. J. Guo and D. J. Brady, "Fabrication of high-resolution micropolarizer arrays," Opt. Eng. **36,** 2268–2271 (1997).
8. G. P. Nordin, J. T. Meier, P. Deguzman, B. Barbour, and M. W. Jones, "Arrays of infrared micropolarizers," In *Diffractive Optics and Micro-Optics*, OSA Technical Digest Series **10,** 133–135 (Optical Society of America, Washington DC, 1998).
9. K. Hirayama, E. N. Glytsis, and T. K. Gaylord, "Rigorous electromagnetic analysis of diffraction by finite-number-of-periods gratings," Jour. Opt. Soc. Am. A **14,** 907–917 (1997).
10. K. Hirayama, E. N. Glytsis, T. K. Gaylord, and D. W. Wilson, "Rigorous electromagnetic analysis of diffractive cylindrical lenses," J. Opt. Soc. Am. A **13,** 2219–2231 (1996).
11. D. W. Prather, M. S. Mirotznik, and J. N. Mait, "Boundary integral methods applied to the analysis of diffractive optical elements," J. Opt. Soc. Am. A **14,** 34–43 (1997).
12. E. N. Glytsis, M. E. Harrigtan, K. Hirayama, and T. K. Gaylord, "Collimating cylindrical diffractive lenses: Rigorous electromagnetic analysis and scalar approximation," Appl. Opt. **37,** 34–43 (1998).
13. D. W. Prather, J. N. Mait, M. S. Mirotznik, and J. P. Collins, "Vector-based synthesis of finite aperiodic subwavelength diffractive optical elements," J. Opt. Soc. Am. A **15,** 1599–1607 (1998).
14. A. Wang and A. Prata, Jr., "Lenslet analysis by rigorous vector diffraction theory," J. Opt. Soc. Am. A **12,** 1161–1169 (1995).
15. M. Schmitz and O. Bryngdahl, "Rigorous concept for the design of diffractive microlenses with high numerical apertures," J. Opt. Soc. Am. A **14,** 901–906 (1997).
16. Y.-K. Kok, "General solution to the multiple-metallic-grooves scattering problem: the fast-polarization case," Appl. Opt. **32,** 2573–2581 (1993).
17. Y. S. Kim, H. J. Eom, J. W. Lee, and K. Yoshitomi, "Scattering from multiple slits in a thick conducting plane," Radio Science **30,** 1341–1347 (1995).
18. O. M. Mendez, M. Cahilhac, and R. Petit, "Diffraction of a two-dimensional electromagnetic beam wave by a thick slit pierced in a perfectly conducting screen," J. Opt. Soc. Am. **73,** 328–331 (1983).

19. S. H. Kang, H. J. Eom, and T. J. Park, "TM-scattering from a slit in a thick conducting screen: revisited," IEEE Trans. Microwave Theory Tech. **41,** 895–899 (1993).
20. T. J. Park, S. H. Kang, and H. J. Eom, "TE-scattering from a slit in a thick conducting screen: revisited," IEEE Trans. Antennas Propag. **42,** 112–114 (1994).
21. D. T. Auckland and R. F. Harrington, "Electromagnetic transmission through a filled slit in a conducting plane of finite thickness, TE case," IEEE Trans. Microwave Theory Tech. **MTT-26,** 499–505 (1978).
22. B. Stenkamp, M. Abraham, W. Ehrfeld, E. Knapek, M. Hintermaier, M. T. Gale, and R. Morf, "Grid Polarizer for the Visible Spectral Region," In *Nanofabrication Technologies and Device Integration*, W. Karthe, ed., Proc. SPIE **2213,** 288–296 (Society of Photo-Optical Instrumentation Engineers, Bellingham, Wash., 1994).
23. H. Lochbihler and R. Depine, "Diffraction from highly conducting wire gratings of arbitrary cross-section," J. Mod. Optics **40,** 1273–1298 (1993).

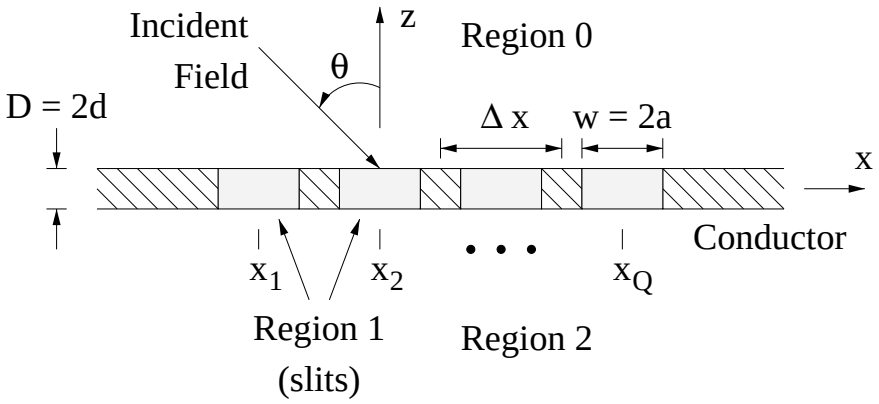

Figure 1: Geometry for a plane wave incident upon the finite-aperture wire polarizer.

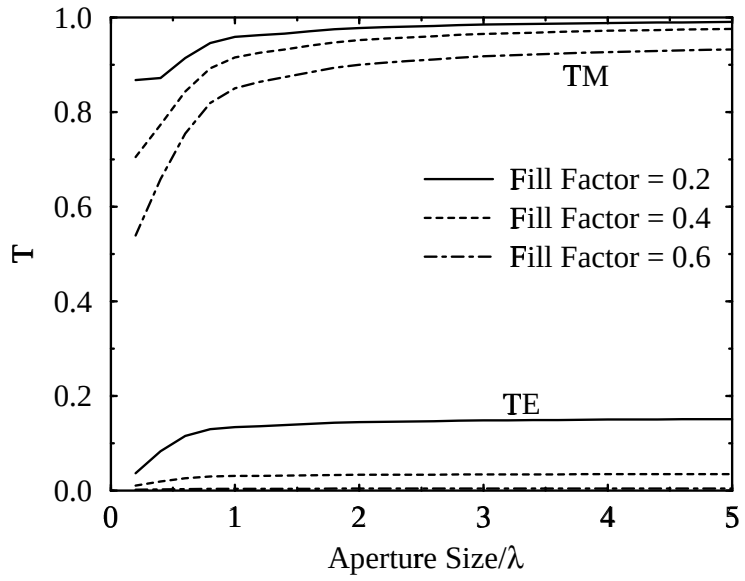

(a)

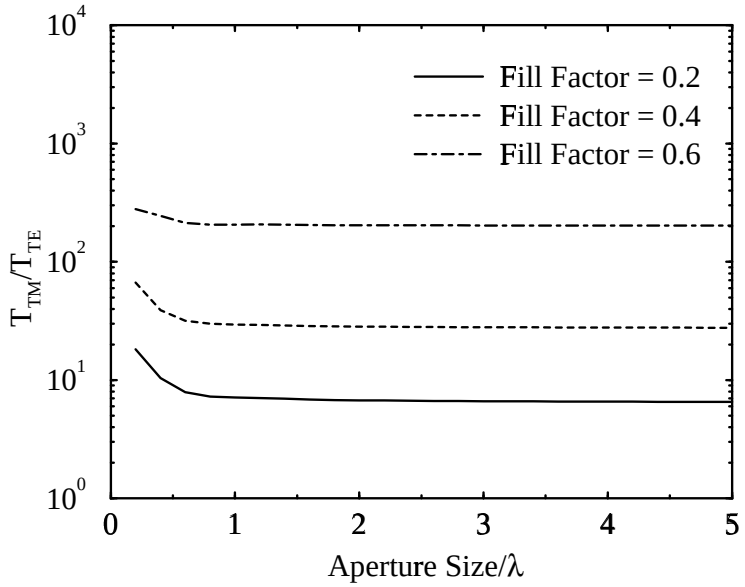

(b)

Figure 2: (a) Transmission coefficient and (b) extinction ratio as a function of aperture size for several values of fill factor ($D = 0$, 5 slits/λ, $N = 5$).

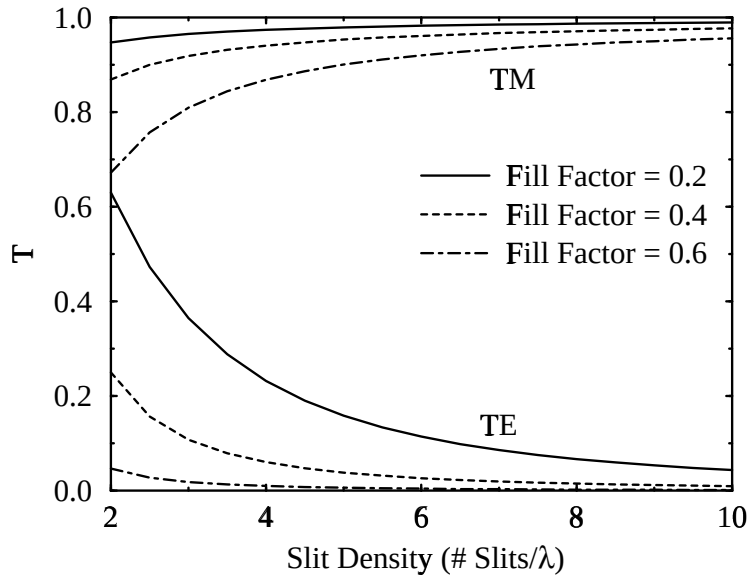

(a)

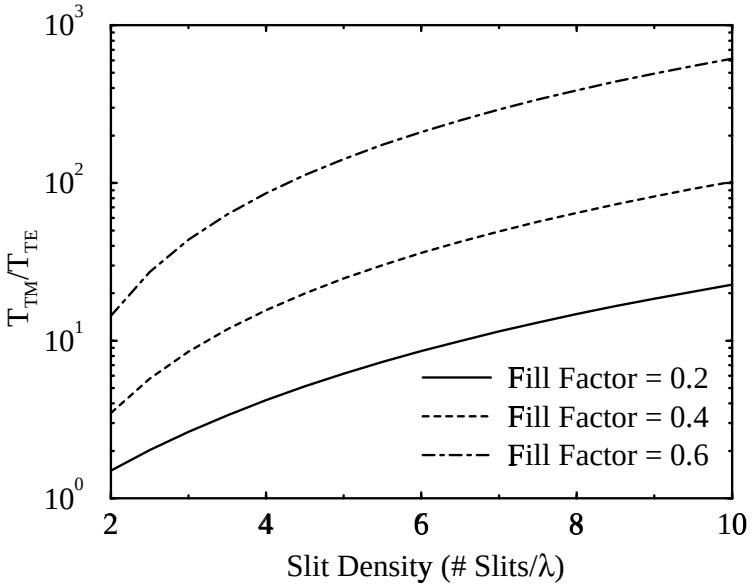

(b)

Figure 3: (a) Transmission coefficient and (b) extinction ratio as a function of slit density for several values of fill factor ($D = 0$, aperture size $= 2\lambda$, $N = 10$).

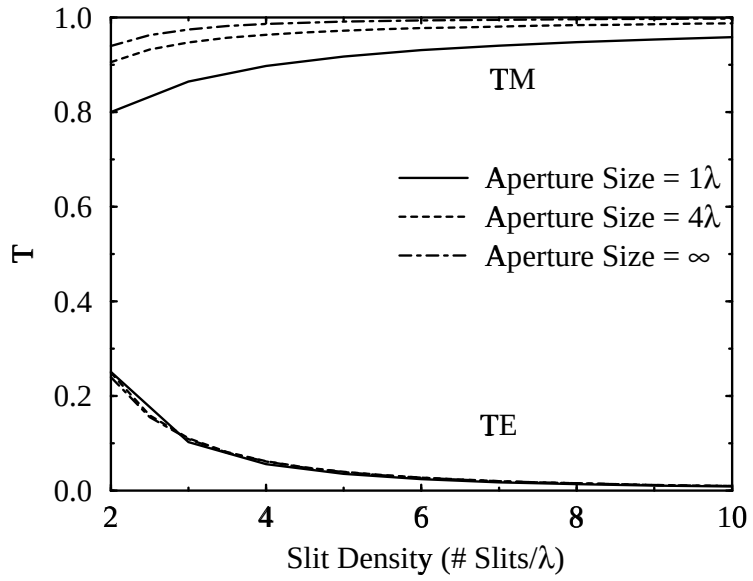

(a)

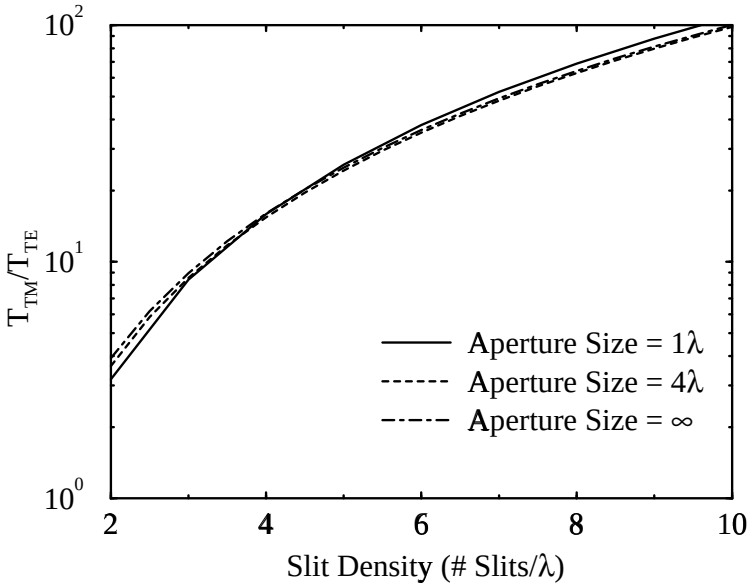

(b)

Figure 4: (a) Transmission coefficient and (b) extinction ratio as a function of slit density for several aperture sizes ($D = 0$, fill factor = 0.4, $N = 10$).

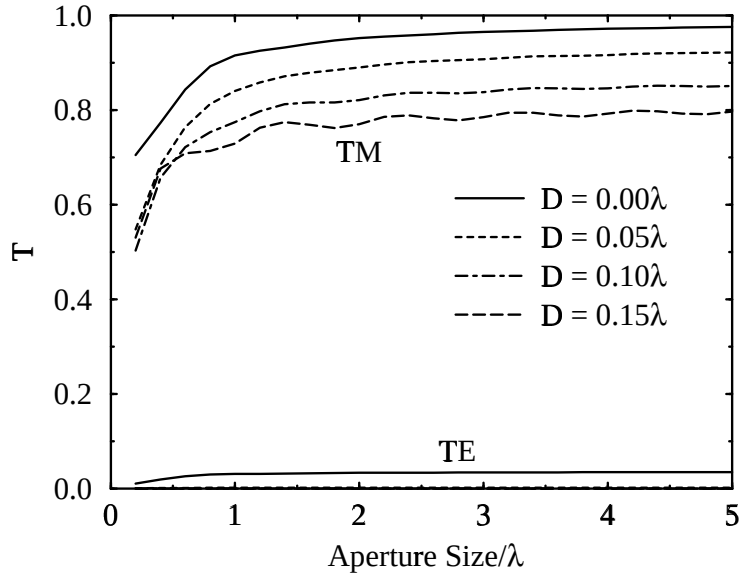

(a)

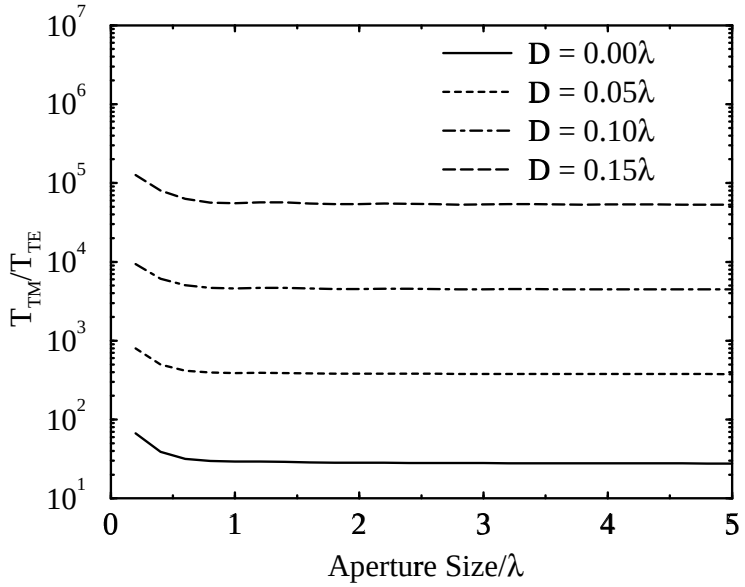

(b)

Figure 5: (a) Transmission coefficient and (b) extinction ratio as a function of aperture size for several values of polarizer thickness (fill factor = 0.4, 5 slits/λ, $N = 5$).

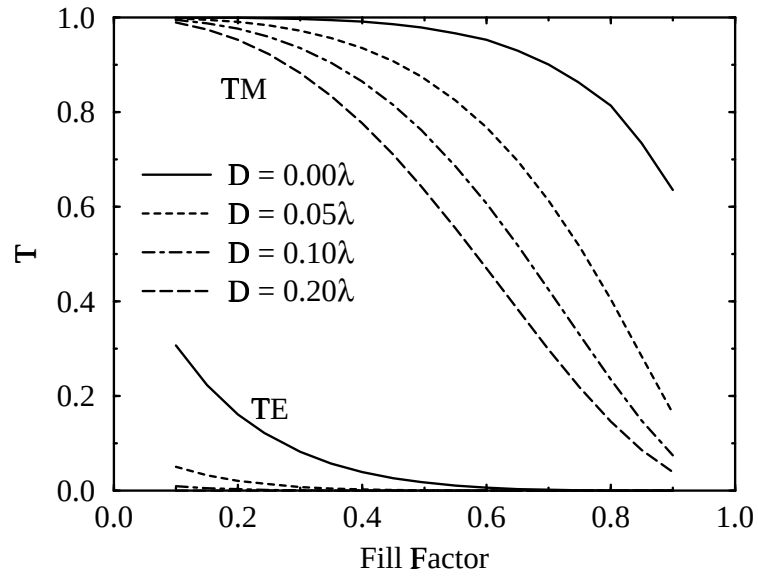

(a)

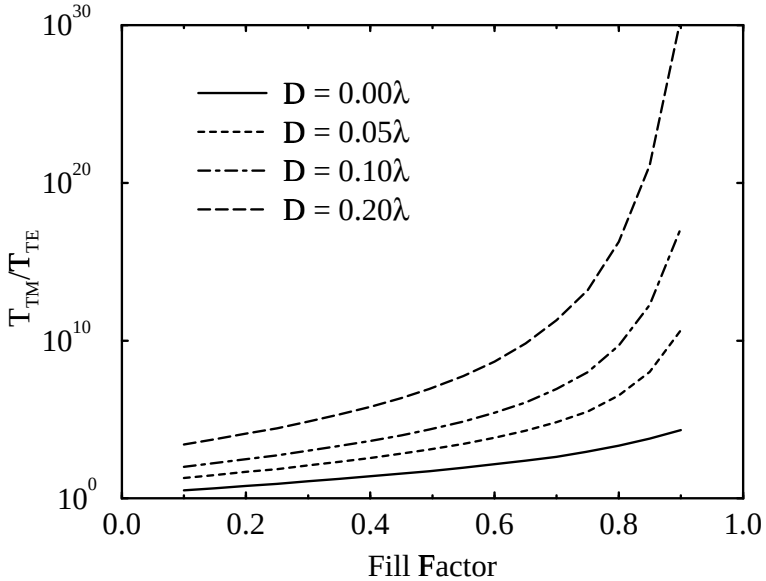

(b)

Figure 6: (a) Transmission coefficient and (b) extinction ratio as a function of fill factor for several values of polarizer thickness (aperture size = ∞, 5 slits/λ, $N = 5$).

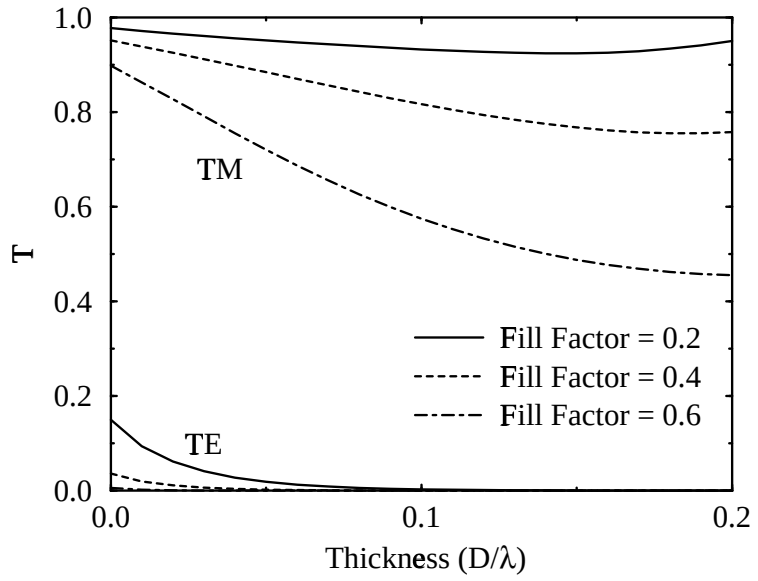

(a)

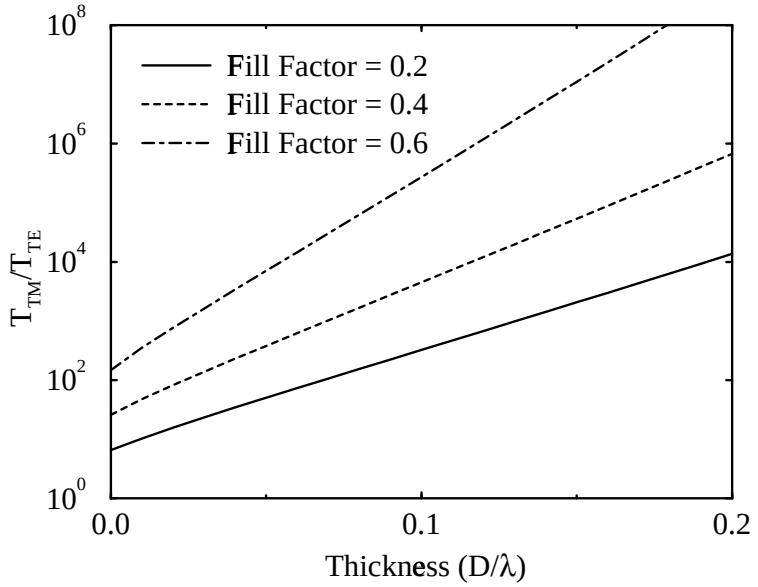

(b)

Figure 7: (a) Transmission coefficient and (b) extinction ratio as a function of polarizer thickness for several values of fill factor (aperture size = 2λ, 5 slits/λ, $N = 5$).

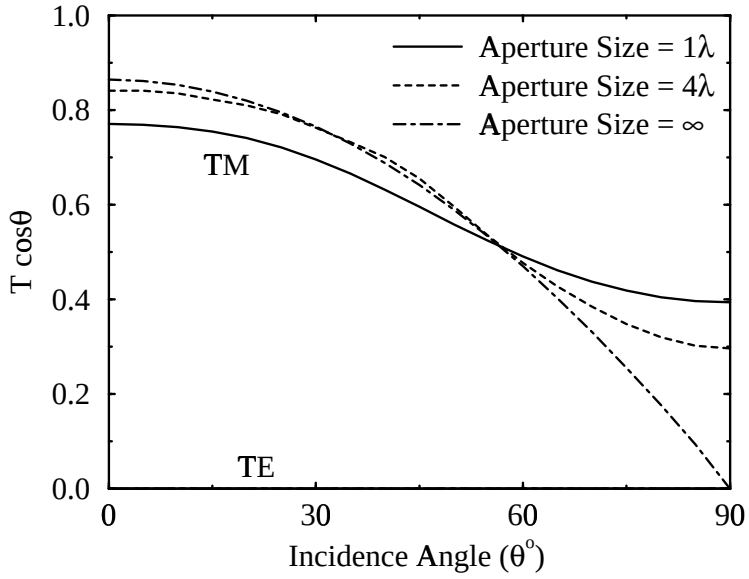

(a)

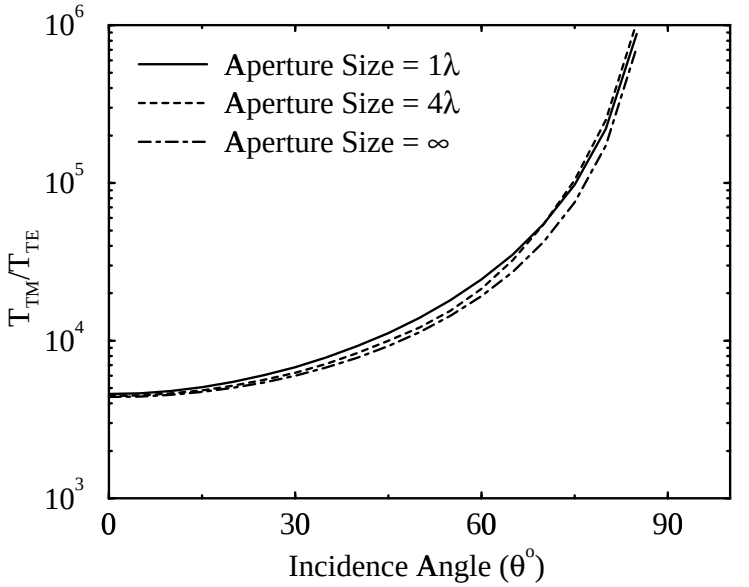

(b)

Figure 8: (a) Normalized transmission coefficient and (b) extinction ratio as a function of plane wave incidence angle for several aperture sizes ($D = 0.1\lambda$, fill factor = 0.4, 5 slits/λ, $N = 5$).

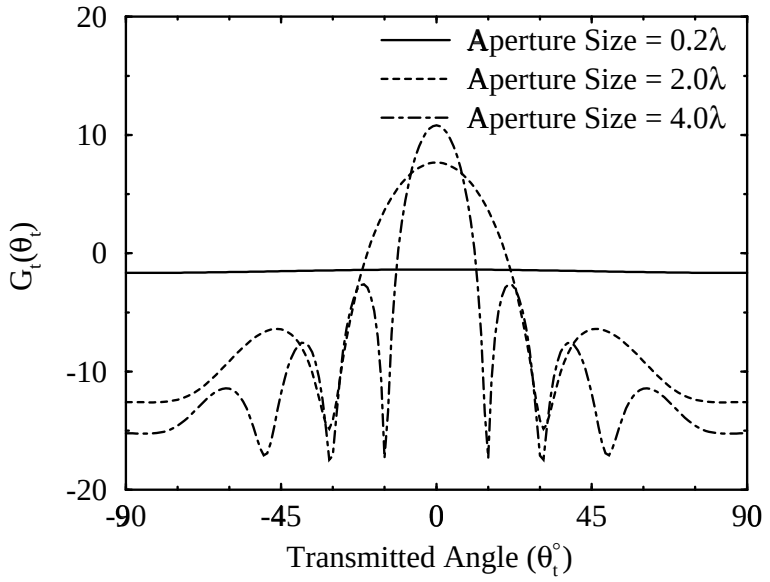

Figure 9: Transmitted diffraction pattern for a polarizer with three different aperture sizes ($D = 0$, 5 slits/λ, fill factor = 0.4, $N = 5$).

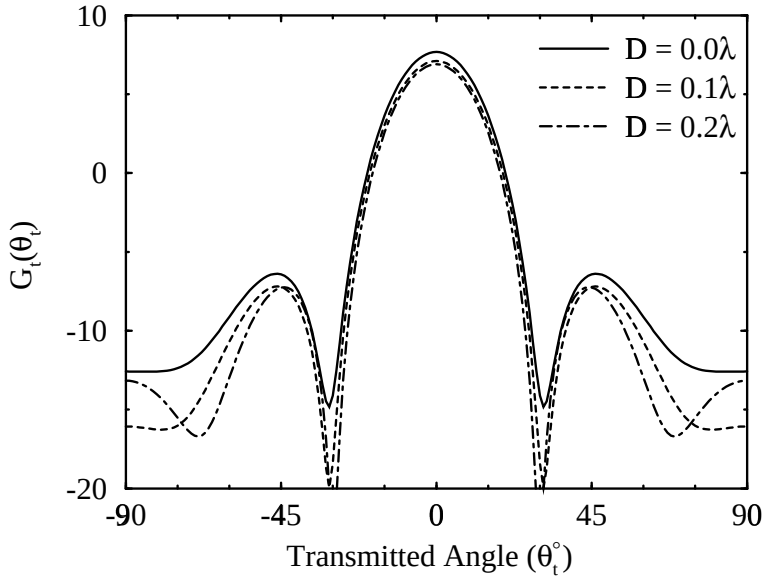

Figure 10: Transmitted diffraction pattern for a polarizer with three different values of thickness (aperture size = 2λ, 5 slits/λ, fill factor = 0.4, $N = 5$).

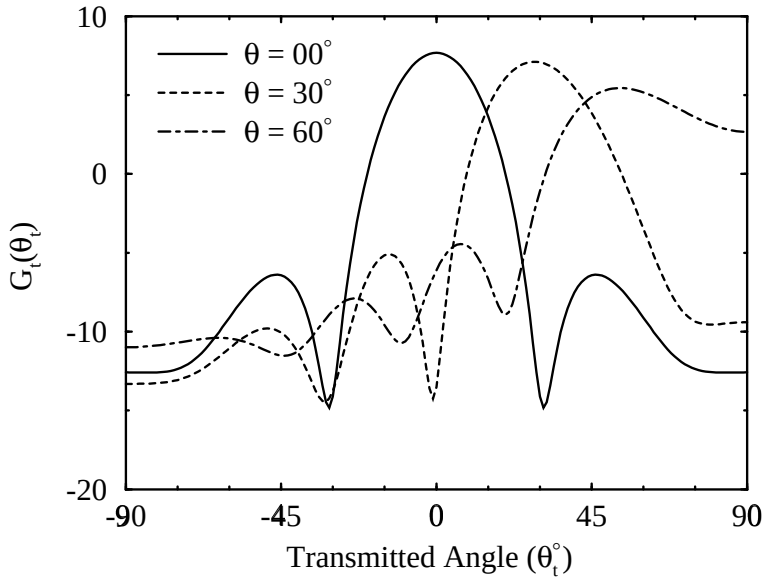

Figure 11: Transmitted diffraction pattern for a polarizer with three different plane wave incidence angles ($D = 0$, aperture size $= 2\lambda$, 5 slits/λ, fill factor $= 0.4$, $N = 5$).